DOI: 10.1002/ejic.201001241

Performance of Dye-Sensitized Solar Cells Based on MWCNT/$TiO_{2-x}N_x$ Nanocomposite Electrodes

Wei Guo,[a] Yihua Shen,[a] Liqiong Wu,[a] Yurong Gao,[a] and Tingli Ma*[a]

Keywords: Solar cells / Metal oxynitrides / Carbon / Nanotubes / Semiconductors / Nanostructures

Multiwall carbon nanotube (MWCNT) fibrils were introduced into $TiO_{2-x}N_x$ photoelectrodes to enhance charge collection efficiency as charge-transport pathways. For comparison, we also synthesized MWCNT/TiO_2 nanocomposites to fabricate dye-sensitized solar cells (DSCs). The effect of MWCNTs on the photovoltaic performance of the DSCs was studied in detail. The performance of DSCs based on MWCNT/$TiO_{2-x}N_x$ differs significantly from that of MWCNT/TiO_2 photoelectrodes. A high energy conversion efficiency of 7.66% was achieved in the dye-sensitized MWCNT/TiO_2 nanocomposites solar cells. The results show that remarkable enhancement of ca. 33% and ca. 40% in the conversion efficiency (η) and short-circuit photocurrent density (J_{sc}), respectively, occurrs for the DSCs based on MWCNT/TiO_2 than those made of pure TiO_2 electrodes. The energy conversion efficiency of DSCs based on $TiO_{2-x}N_x$ electrodes was 6.98%, which is similar to that of MWCNT/$TiO_{2-x}N_x$ DSCs (6.88%–5.17%). We also investigated the charge collection efficiency, electron transport, electron lifetime, and photocurrent transient behavior by electrochemical analysis. The introduced MWCNTs exhibit a smaller sheet resistance and electron transfer resistance, as well as a longer electron lifetime. A 20% enhancement in the charge collection efficiency is achieved in the nanocomposite DSCs.

Introduction

Dye-sensitized solar cells (DSCs) have attracted much attention because of their cost efficiency, simple fabrication process, and high conversion efficiency.[1–3] Many studies have been carried out because of the demand for photovoltaic technologies for large-scale energy production.[4,5] One of the key aspects of DSCs is the mesoporous semiconductor oxide film, which functions as a dye-sensitizer absorber and electron collector that collects electrons to the outer circuit. During the illumination of solar cells, electrons generated by photoexcited dye molecules are injected into the conduction band of the oxide. Although most electrons can be efficiently collected, recombination with triiodide and excited dyes can still occur for certain electrons before reaching the outer circuit. This is one of the main losses in potential, which results in the failure of achieving a higher energy conversion efficiency. Therefore, it is important to improve the charge collection efficiency of the semiconductor oxide.

Previous studies have reported the unique geometry and excellent electronic, thermal, and mechanical properties of carbon nanotubes (CNTs).[6,7] Meanwhile, the incorporation of CNTs into TiO_2, which maximizes the advantages of both materials, has become the subject of much research.[8] Studies have been performed on the introduction of CNTs into the electrode of DSCs and organic solar cells.[9–17] Kamat et al. presented the beneficial role of the single-wall CNTs as conducting scaffold to facilitate charge collection and electron transport in nanostructured semiconductor films.[11,12] Previous studies have reported that direct mixing of CNTs with commercial P25 or TiO_2 anatase nanopowder leads to serious CNT aggregation, thereby suppressing photovoltaic performance. The energy conversion efficiency of those DSCs range from 4.04–4.97%.[10,15,18] Recently, the hydrothermal method has also been used to synthesize homogeneous multiwall carbon nanotube (MWCNTs)/TiO_2 nanocomposites. DSCs based on these nanocomposites have achieved an energy conversion efficiency ranging from 4.62–7.37%. However, the mixed crystal of the rutile and brookite phases appeared in the nanocomposites.[14,17] These studies have demonstrated that CNTs can improve conductivity, increase the surface area of electrodes, and enhance the energy conversion efficiency of photovoltaic devices. Therefore, the use of CNTs to enhance the photovoltaic performance of solar cells is a promising and worthwhile research endeavor. However, good interaction between CNTs and TiO_2 is essential. The flow of photogenerated electrons can then be regularly guided to improve charge separation and carrier transport. Recently, Li et al. have reported a novel architecture of DSCs based on TiO_2-coated, vertically aligned nanofiber arrays. However, although the architecture is promising, it needs to be optimized since the energy conversion efficiency of such DSCs is only about 1.09%.[16]

[a] State Key Laboratory of Fine Chemicals, Dalian University of Technology,
Dalian 116024, P. R. China
Fax: +86-411-62253767
E-mail: tinglima@dlut.edu.cn

Although many reports on CNTs/TiO_2 have been published, to the best of our knowledge, DSCs based on the photoelectrode of CNTs/$TiO_{2-x}N_x$ have not been reported so far. In our previous work, we have successfully introduced N-doped TiO_2 to the photoelectrodes of DSCs.[19] In another study, N-doped TiO_2 has been introduced to quantum-dot solar cells.[20] An enhanced photocurrent and retarded electron recombination has been observed in DSCs.[21–23] Therefore, we attempted to use MWCNT/$TiO_{2-x}N_x$ nanocomposites as photoelectrodes to enhance electron transfer and collection, which can further improve the photovoltaic performance of DSCs.

In the present work, we introduced graphite fibrils of MWCNTs into nanostructured TiO_2 materials. The one-dimensional network is expected to assist electron transport to the collecting photoelectrode surface in the DSCs. A modified sol–gel method has been used to synthesize MWCNT/TiO_2 nanocomposites. We have found interesting results upon the introduction of MWCNT/$TiO_{2-x}N_x$ nanocomposites as new semiconductor nanocomposites for DSCs. The properties of the nanocomposites and films were investigated by X-ray diffraction (XRD) and scanning electron microscopy (SEM). The effect of MWCNTs on the photocurrent–voltage characterization of DSCs was studied by photoelectrochemical analysis. We further investigated the role of MWCNTs in charge collection efficiency, electron transport, and electron lifetime.

Results and Discussions

Characterization of Microstructure and Phase Structure

The fibrous-type MWCNTs used in this work possess high purity and a uniform diameter distribution as reported by Matsuo et al.[24] The peak of the Raman-allowed phonon mode, E_{2g}, at 1582 cm^{-1} is not very sharp and its intensity at 1345 cm^{-1} is high, which occurs through the disorder-induced phonon mode as a result of the infinite size of the crystals and defects.[25] This indicates that MWCNTs have a low degree of graphitization. Acid-treatment of MWCNTs can produce finely dispersed MWCNTs and introduce carboxylic acid groups on the surface of MWCNTs.[26] We expect that the carboxyl acid group can serve as a good connection between MWCNTs and TiO_2. The microstructure of MWCNTs after acid and thermal treatment at 450 °C for 1 h can be observed in Figure 1, which shows that the MWCNTs maintain its fibrous nature and has excellent thermostability.

The microstructures of MWCNT/TiO_2 films from the SEM image, represented by the 0.06-MT and 0.50-MT films, are shown in Figure 1 [X-MT is used to designate MWCNT/TiO_2 nanocomposites with different weight ratios (X relates to the weight ratio of the MWCNTs in the nanocomposite)]. The nanocomposite electrodes exhibit nanoporous nanostructures. No incorporated MWCNTs fibrils were observed on the surface of the nanocomposite film for a MWCNT content of up to 0.06%. This implies that

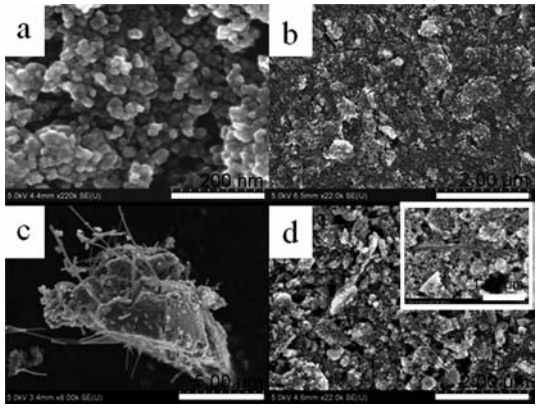

Figure 1. SEM image (a) and (b) 0.06-MT films; (c) 0.50-MT nanocomposite powder after sintering at 450 °C for 1 h; (d) 0.50-MT films.

MWCNTs are entirely covered by bulk TiO_2. However, as the content of the MWCNTs is increased to 0.50%, MWCNT fibrils run through the nanocomposite powder (Figure 1c). We can also observe the bare MWCNT fibril going through the films (the inset in Figure 1d). The surface morphology of the nanocomposite electrode also varies with the MWCNT content (Figure 1b, d). As the content of the MWCNTs increases from 0.06 to 0.50%, a more porous nanostructure is formed, which can be ascribed to the contribution of the MWCNTs. Furthermore, we can see obvious aggregation of TiO_2 in the films. As MWCNT fibers were introduced into TiO_2 during hydrolysis of TTIP, it was found that the MWCNTs can also act as nucleation sites, which leads to the aggregation of the TiO_2 particles.

Figure 2 shows the XRD patterns of TiO_2, $TiO_{2-x}N_x$, and 0.50-MT. The peaks can be attributed to anatase TiO_2. However, we cannot observe the peaks at 2θ positions of 26.0° and 43.4°, which are characteristic of carbon materials.[27] The reason for this is that the intensity of the main peak for anatase (101) at 25.4° is quite high and overlaps the main peaks of the MWCNTs. In addition, the small amount of MWCNTs makes it difficult to identify their characteristic peaks. The crystallite sizes for TiO_2, $TiO_{2-x}N_x$, and 0.50-MT are 15.25, 17.85, and 16.47 nm, respectively. These calculated results are consistent with

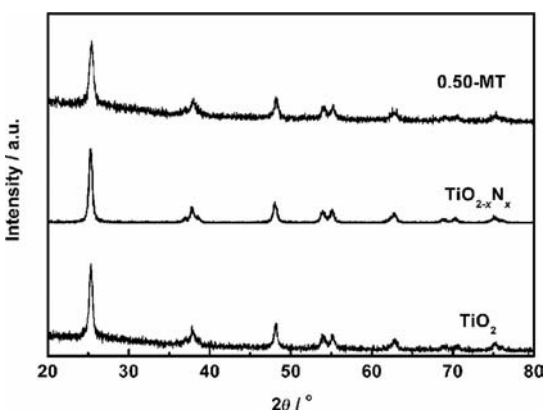

Figure 2. X-ray diffraction patterns.

those from the SEM images (Figure 1a), which indicates that the introduction of the MWCNTs does not affect the crystallite size of TiO_2.

Photovoltaic Performance of DSCs

We assembled the dye-sensitized solar cells with the nanocomposite electrodes. Figure 3a shows the photovoltaic performance of the DSCs based on the MWCNT/TiO_2 electrodes containing various amounts of MWCNTs. The detailed data are listed in Table 1. Based on the pure TiO_2 electrode, the energy conversion efficiency (η) of the solar cell is 5.78%. When the content of the MWCNTs increases from 0.01 to 0.06%, the value of the short-circuit photocurrent density (J_{sc}) significantly increases by ca. 40% from 10.91 to 15.27 mA cm^{-2}. The energy conversion efficiency also improves by ca. 33% from 5.78 to 7.66%. The improvement in η and J_{sc} apparently exceeds measuring errors, which further demonstrates the role that MWCNTs play in photoelectrodes. However, as the content of MWCNTs is further increased to 0.50%, the energy conversion efficiency of the DSCs decreases to 3.87%, which is even lower than that of DSCs based on the pure TiO_2 electrode. The value of J_{sc} decreases from 15.27 to 8.30 mA cm^{-2}, and the value of the open-circuit voltage (V_{oc}) decreases from 0.752 to 0.661 V.

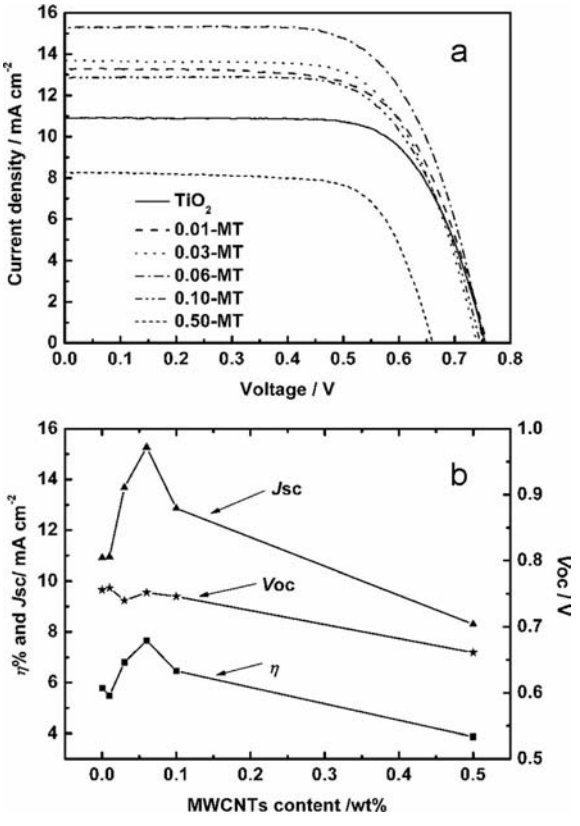

Figure 3. (a) Photocurrent–voltage characteristics of DSCs based on MWCNT/TiO_2 electrodes; (b) effect of the different MWCNT content on the photovoltaic performance parameters of the DSCs.

Table 1. Photovoltaic performance and electron lifetime of the DSCs based on MWCNT/TiO_2 nanocomposite electrodes. FF = fill factor.

Sample	V_{oc} [V]	J_{sc} [mA cm^{-2}]	FF [%]	η [%]	τ_e [ms]
TiO_2	0.756	10.91	70.1	5.78	19.4
0.01-MT	0.759	10.95	66.0	5.49	–
0.03-MT	0.740	13.68	67.2	6.80	14.8
0.06-MT	0.752	15.27	66.7	7.66	13.8
0.10-MT	0.746	12.86	67.3	6.46	21.0
0.50-MT	0.661	8.30	70.5	3.87	18.7

The effect of the content of the MWCNTs on the photovoltaic performance of the DSCs is shown in Figure 3b. As can be seen, there exists an optimum value for the content of the MWCNTs in the nanocomposite electrode. The optimum content of the MWCNTs varies with the method of incorporation into TiO_2.[10,13–15,17,18] In our case, the optimum content of the MWCNTs is 0.06%. The photocurrent is first enhanced and then weakens as the content of the MWCNTs increases. Although the MWCNT fibrils play an important role in the electron transport pathway, more MWCNTs can cause light-harvesting competition between the dye molecules and the MWCNTs.[14] Moreover, V_{oc} does not change at first; it decreases as the content of the MWCNTs increases to 0.50%. The Fermi equilibrium between TiO_2 and CNTs causes V_{oc} to decrease.[11] Moreover, a higher recombination rate generally leads to a smaller open-circuit voltage.[28] In this work, recombination sites can come from: (a) the heterogeneous interfaces between the CNTs and the bulk TiO_2[11] and (b) the bare MWCNTs not covered by TiO_2 and dye molecules (Figure 1c).[18] More recombination sites may also be the reason for the lower V_{oc} value.

To further clarify the higher J_{sc} value of the DSCs based on the MWCNT/TiO_2 nanocomposite electrodes, action spectra were measured by monitoring the photocurrent at different incident wavelengths (Figure 4). We can clearly observe a significant enhancement in the incident photo-to-current conversion efficiency (IPCE) for the 0.03-MT and 0.06-MT DSCs in the range 350–650 nm. As the content of the MWCNTs increases to 0.50%, the IPCE value decreases

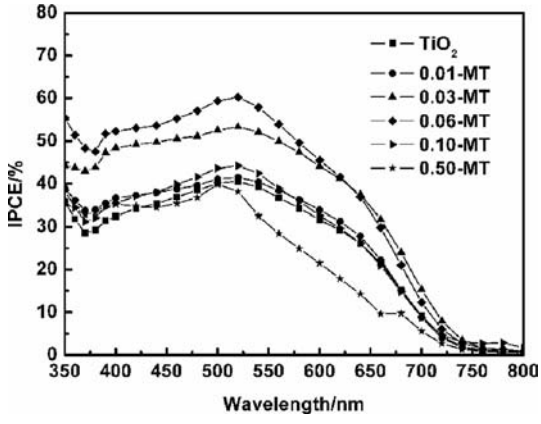

Figure 4. Action spectra of the DSCs based on the MWCNT/TiO_2 electrodes.

dramatically in the range 500–700 nm, which thereby demonstrates the light-harvesting competition between the dye and the MWCNTs.[14]

In our previous work, we developed highly efficient solar cells based on nitrogen-doped TiO_2 electrodes.[19] According to work on MWCNT/TiO_2 nanocomposite electrodes, the overall performance of DSCs can be expected to improve further by incorporating MWCNTs into nitrogen-doped TiO_2. Therefore, we carried out another set of experiments on DSCs based on MWCNT/$TiO_{2-x}N_x$ nanocomposite electrodes. Surprisingly, we obtained a suppressed photovoltaic performance. The nitrogen content in the N-doped TiO_2 is 0.43% based on X-ray photoelectron spectroscopy. We can see from the J–V curves and the detailed data of the DSCs based on MWCNT/$TiO_{2-x}N_x$ in Figure 5a and Table 2 that the energy conversion efficiency of DSCs based on the $TiO_{2-x}N_x$ electrode is 6.98%, which is higher than that of DSCs based on pure TiO_2 electrodes (5.52%). The reason for the improvement in the photovoltaic performance in the DSCs based on nitrogen-doped TiO_2 has been discussed in our previous work.[19,29] However, in DSCs based on MWCNT/$TiO_{2-x}N_x$ electrodes, the DSCs give similar photovoltaic performance when the content of the MWCNTs increases from 0.03 to 0.06%; the energy conversion efficiency ranges from 6.98–6.57%. The J_{sc} and V_{oc} values do not show an obvious decrease in their respective levels. When the content of the MWCNTs is increased to 0.50%, the energy conversion efficiency decreases to 5.17%. In detail, the J_{sc} value decreases by 28% from 13.10 to 10.19 mA cm^{-2} and V_{oc} decreases from 0.801 to 0.738 V. The reason for the lower J_{sc} value has been discussed above.

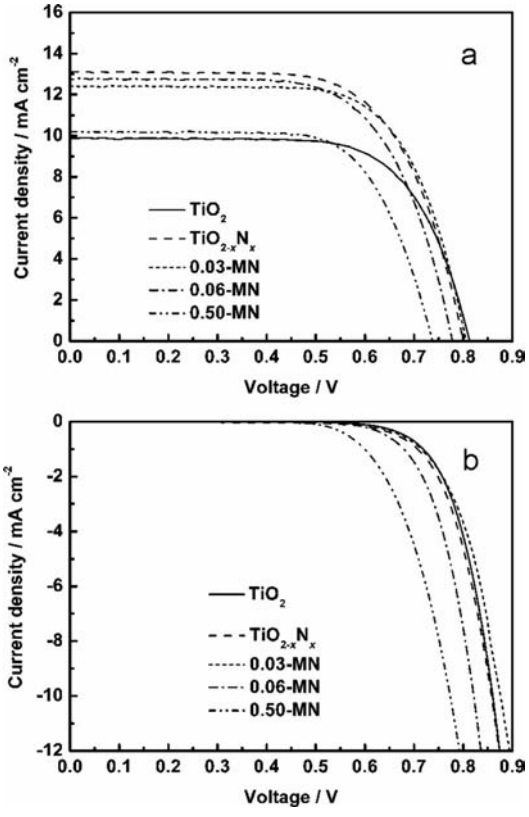

Figure 5. (a) Photocurrent–voltage characteristics of DSCs based on MWCNT/$TiO_{2-x}N_x$ electrodes; (b) Photocurrent–voltage characteristics of the DSCs in the dark.

Table 2. Photovoltaic performance of DSCs based on MWCNT/$TiO_{2-x}N_x$ electrodes. FF = fill factor.

Sample	V_{oc} [V]	J_{sc} [mA cm^{-2}]	FF [%]	η [%]
TiO_2	0.814	9.88	68.6	5.52
$TiO_{2-x}N_x$	0.801	13.10	66.6	6.98
0.03-MN	0.807	12.41	68.7	6.88
0.06-MN	0.779	12.74	66.2	6.57
0.50-MN	0.738	10.19	68.7	5.17

We further investigated the reasons behind the interesting photovoltaic performance of the DSCs based on the MWCNT/$TiO_{2-x}N_x$ electrodes. Dark current is an important parameter for the evaluation of the electron recombination between the photoinjected electrons and I_3^- in the electrolyte. A smaller dark current is critical in obtaining a high V_{oc} value.[30] In this work, we studied the dark current of the DSCs assembled with the pure TiO_2, $TiO_{2-x}N_x$, and MWCNT/$TiO_{2-x}N_x$ electrodes. The results are shown in Figure 5b. When nitrogen-doped TiO_2 DSCs are compared with pure TiO_2 DSCs, the former exhibit a smaller dark current. However, after assembling the MWCNT/$TiO_{2-x}N_x$ electrodes with DSCs, the dark current of the solar cells, except that of the 0.03-MN DSC, was much larger than those of nitrogen-doped DSCs and pure TiO_2 DSCs [X-MN is used to designate MWCNT/$TiO_{2-x}N_x$ nanocomposites with different weight ratios (X relates to the weight ratio of MWCNTs in the nanocomposite]. Therefore, the larger dark current is one of the reasons for the lower photovoltage, which suppresses the photovoltaic performance of the solar cells.

Photocurrent Transient Analysis

More recombination sites also lead to lower V_{oc} values; thus, we performed photocurrent transient measurements by electrochemical methods. When the photoanodes of the TiO_2 films are excited by UV light ($E_g > 3.2$ eV), the generated anodic photocurrent indicates that charge separation occurs on the surface of the electrode. The magnitude of the photocurrent represents the charge collection efficiency of the electrode surface.[11] The thickness of the film was controlled to obtain nearly equal amounts of TiO_2 particles that undergo photocurrent generation and charge separation. The electrodes generate photocurrent immediately after irradiation and show reproducible responses to ON–OFF cycles. Figure 6A shows the photocurrent transient behavior generated under simulated solar light. It can be clearly seen that the 0.06-MT electrode (0.30 cm^2) possesses an enhanced photocurrent, which indicates that a promotion in charge separation and charge transfer has been achieved by introducing the MWCNTs. In Figure 6B, we compare the short-circuit photocurrent generation at the

TiO_2, $TiO_{2-x}N_x$, and MWCNT/$TiO_{2-x}N_x$ electrodes (0.16 cm^2) with varying amounts of MWCNTs. It can be observed that the $TiO_{2-x}N_x$ electrode shows the largest photocurrent responses among the three kinds of electrodes. The results are consistent with those of previous works.[21,31] However, the 0.06-MN and 0.50-MN electrodes exhibit weakened photocurrent, which indicates that poorer charge separation and collection occurs in the two electrodes relative to the other three. Therefore, we can conclude that more recombination sites evidently exist in the MWCNT/$TiO_{2-x}N_x$ electrode.

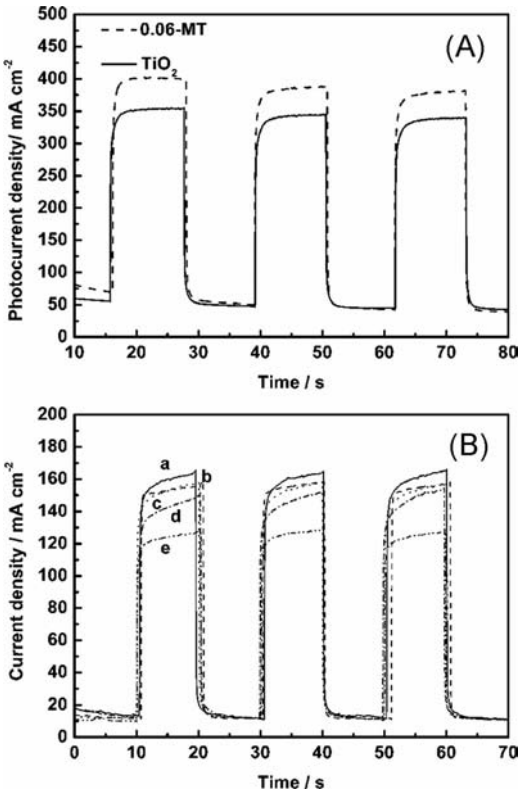

Figure 6. Photocurrent transient behavior generated during photoirradation under simulated solar light. (A) TiO_2 and 0.06-MT electrodes, area 0.30 cm^{-2}; (B) $TiO_{2-x}N_x$ and MWCNT/$TiO_{2-x}N_x$ electrodes, area 0.16 cm^{-2} (a) $TiO_{2-x}N_x$; (b) TiO_2; (c) 0.03-MN; (d) 0.06-MN; (e) 0.50-MN.

Electrochemical Impedance Analysis

There is a need to gain a better understanding of the electronic and ionic processes occurring in DSCs based on MWCNT/TiO_2 and MWCNT/$TiO_{2-x}N_x$ electrodes. Electrochemical impedance spectroscopy is a powerful steady-state technique that has been widely used to study the kinetics of electrochemical and photoelectrochemical processes in DSCs. Key parameters characterizing electron transport, back reaction, and charge transfer at a counter electrode can be extracted by applying appropriate equivalent circuits.[32] The Nyquist diagram typically features three semicircles in order of increasing frequency that correspond to the Nernst diffusion within the electrolyte, electron transport at the oxide/electrolyte interface, and the redox reaction at the platinum counter electrode.[33] Our present study mainly focuses on semiconductor photoanodes. Impedance due to electron transfer from the conduction band of the mesoscopic film to the triiodide ions in the electrolyte and the back reaction at the TiO_2/electrolyte interface, presented by the semicircle in intermediate-frequency regime, are our major concerns in this research. The mean electron lifetime ($\tau_{n,EIS}$) in TiO_2 can be estimated from the following Equation (1):

$$\tau_{n,EIS} = (2\pi f_{max})^{-1} \quad (1)$$

where f_{max} is the frequency at the top of the intermediate-frequency arc.[33,34] The sheet resistance (R_s) of the cell was measured when electrons were transported through the devices in the high-frequency range, exceeding 10^6 Hz.

Figure 7 shows the electrochemical impedance spectra of DSCs based on TiO_2 and MWCNT/TiO_2 electrodes measured at a forward bias of 0.75 V in the dark. Generally, R_s values for 0.03-MT and 0.06-MT are smaller than that of pure TiO_2. This result indicates that the R_s of DSCs becomes smaller with the incorporation of MWCNTs. With regard to the semicircle in the middle-frequency range of the electrochemical spectra, electron transfer resistance first decreases then increases with an increase in the content of MWCNTs. The 0.06-MT DSCs, which yield the highest en-

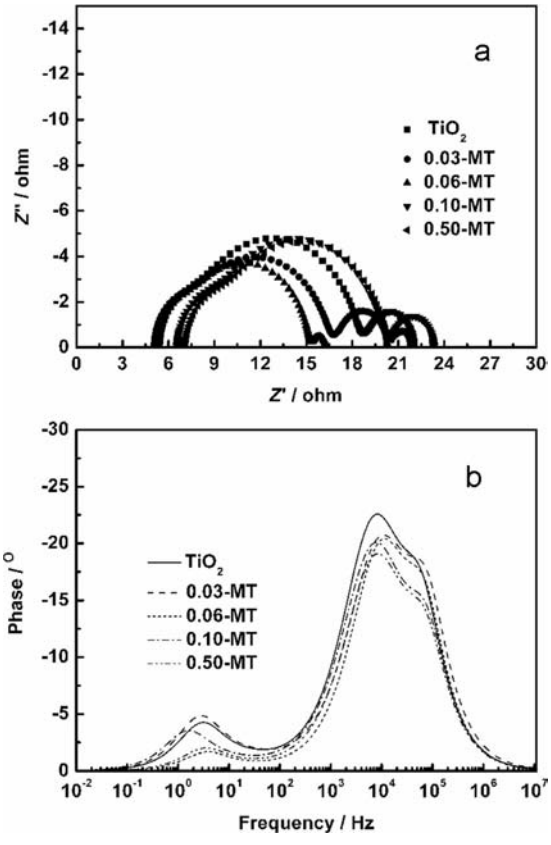

Figure 7. Electrochemical impedance spectra of DSCs based on MWCNT/TiO_2 electrodes measured at a forward bias of 0.75 V in the dark. (a) Nyquist plot and (b) Bode phase plot.

ergy conversion efficiency, give the smallest semicircle. As the content of MWCNTs increases, electron transfer resistance became larger. This may be due to more recombination sites, as similarly seen for the photovoltaic performance of DSCs. We also studied the electron lifetime (τ_e) of the DSCs. Details are listed in Table 1. As can be seen from the electrochemical impedance spectra, f_{max} first shifts to the left then to the right, which indicates that the electron lifetime first becomes shorter then longer by increasing the content of MWCNTs.

The kinetics of electron injection, transport, and lifetime has been studied previously. The timescale for electron injection has been found to be in the range of picoseconds,[35] and that of the electron lifetime in the several milliseconds to seconds.[36] The photoinjected electrons move through the network of interconnected TiO_2 nanoparticles, usually a random walk process, and undergo lots of trapping and detrapping events. During this transport of electrons to the outer circuit, the electrons may be lost by back-electron-transfer to the triiodide species in the redox electrolyte. Competition between electron collection and back-electron-transfer determines the performance of DSCs. Ideally, all injected electrons should be collected without loss.[37] Therefore, a smaller electron transfer resistance, an efficient electron collection, and a longer lifetime are necessary for the improvement of the photovoltaic performance of DSCs.

It is interesting to identify the reason behind the suppressed photovoltaic performance of MN-DSCs. Table 3 and Figure 8 show the electrochemical impedance spectra of DSCs based on the $TiO_{2-x}N_x$ and MWCNT/$TiO_{2-x}N_x$ electrodes measured at a forward bias of 0.75 V in the dark. When the N-doped DSCs are compared with the MN-DSCs, a decrease in R_s is observed with an increase in the content of MWCNTs. Meanwhile, the resistance of the MN electrodes (R_t) decreases with an increase in the content of MWCNTs. The reduced R_s and R_t are apparently ascribed to the incorporation of MWCNT fibrils. However, electron transfer resistance (R_{ct}) increases with an increase in the content of MWCNTs. N-doped DSCs, which yield the highest energy conversion efficiency, result in the smallest semicircle in the middle frequency range of the electrochemical impedance spectra. The mean electron lifetime ($\tau_{n,EIS}$) in TiO_2 was also calculated and is listed in Table 3. The f_{max} of N-doped DSC shifts to the left relative to that of DSCs based on TiO_2, whereas f_{max} of MN-DSCs shifts to the right relative to that of N-doped DSCs, which indicates that the electron lifetime in N-doped DSCs and MN-DSCs is relatively longer than that in DSCs based on pure TiO_2 electrodes. Therefore, electron transfer resistance, rather than electron lifetime, is the main reason for the suppressed photovoltaic performance.

Whether or not the incorporation of MWCNTs can guide the flow of electrons to the outer circuits should be confirmed. Thus, we further investigated the charge collection efficiency in the MN-DSCs. Grätzel et al. analyzed the charge collection and charge extraction in dye-sensitized solar cells.[38] They proposed that the charge collection rate at the FTO contact is expressed as Equation (2).

Table 3. Electrochemical impedance data of DSCs based on MWCNT/$TiO_{2-x}N_x$ electrodes.

Sample	R_s [ohm][a]	$R_{t(TiO2)}$ [ohm][b]	R_{ct} [ohm] [c]	τ_e [ms][d]	η_{cc} [%] [e]
TiO_2	3.79	5.30	17.49	19.6	76.7
$TiO_{2-x}N_x$	7.71	5.23	14.68	24.9	73.7
0.03-MN	7.08	4.83	16.57	19.4	77.4
0.06-MN	5.36	3.66	16.38	26.6	81.7
0.50-MN	3.65	2.49	19.01	21.1	88.4

[a] Sheet resistance. [b] Electron transport resistance in the TiO_2 films. [c] Interfacial electron recombination resistance. [d] Electron lifetime. [e] Charge collection efficiency.

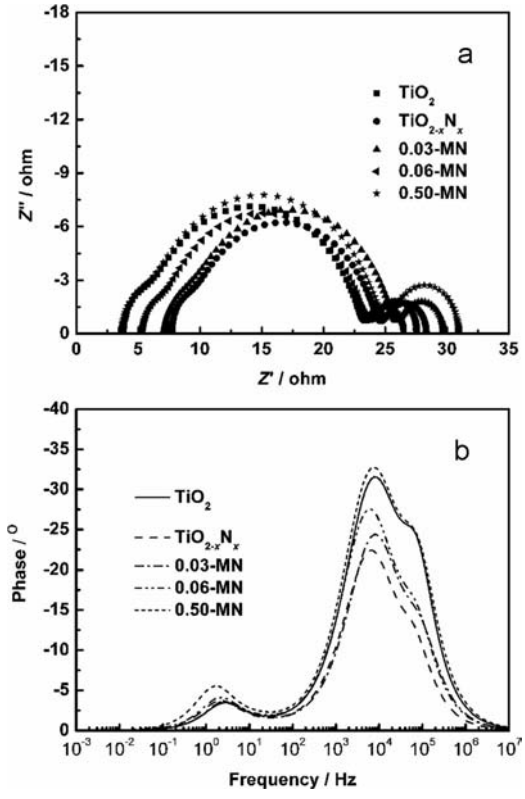

Figure 8. Electrochemical impedance spectra of DSCs based on MWCNT/$TiO_{2-x}N_x$ electrodes measured at a forward bias of 0.75 V in the dark. (a) Nyquist plot and (b) Bode phase plot.

$$\frac{1}{\tau_{cc}}=\frac{1}{\tau_t}-\frac{1}{\tau_r} \quad (2)$$

where τ_{cc}, τ_t, and τ_r represent the time constants for charge collection, transport, and recombination, respectively. Therefore, the charge collection efficiency can be written as Equation (3).

$$\eta_{cc}=\frac{1}{\tau_{cc}}/\left(\frac{1}{\tau_{cc}}+\frac{1}{\tau_r}\right)=1-\frac{R_t}{R_{ct}+R_t} \quad (3)$$

We can extract R_t and R_{ct} by applying the equivalent circuits.[28] The values of η_{cc} are shown in Table 3. The results reveal that incorporation of the MWCNTs can im-

prove the charge collection efficiency by ca. 21% from 73.7 to 88.4%. Therefore, the one-dimensional network of nanocomposites provides an efficient electron pathway and enhances the charge collection efficiency.

We can conclude that the introduction of carbon nanostructures into DSCs improves the conductivity of the semiconductor films and leads to the collection of electrons efficiently. However, it is important to disperse well-organized carbon nanotubes to realize the uniform collection of electrons. Meanwhile, the reduction of heterogeneous interfaces is essential for making the carbon nanostructures play a better role. The type of CNT materials and the proper length of the nanostructure also affect charge collection and electron transport; these can be the topics of future work.

Conclusions

Fibrous-type MWCNT fibrils were introduced into TiO_2 photoelectrodes of DSCs to enhance electron transport and charge collection efficiency. Nanocomposites of MWCNT/TiO_2 and MWCNT/$TiO_{2-x}N_x$ were synthesized by a modified acid-catalyzed method. The results show that a significantly enhanced energy conversion efficiency of ca. 33% and an improvement of the J_{sc} value by ca. 40% was achieved by the DSCs based on MWCNT/TiO_2 nanocomposite electrodes. Moreover, introduction of the MWCNTs contributed to a smaller sheet resistance, longer electron lifetime, and smaller electron transfer resistance. The suppressed photovoltaic performance of the DSCs based on novel MWCNT/$TiO_{2-x}N_x$ nanocomposites is mainly due to a larger electron transfer resistance and to more recombination sites. A lower photovoltage may also be due to a larger dark current and to more recombination sites. A 20% enhancement of the charge collection efficiency was achieved in the nanocomposite DSCs. This study has also given clear evidence on the improvement of the charge collection efficiency in dye-sensitized solar cells based on MWCNT nanocomposites.

Experimental Section

Materials: Fibrous-type MWCNTs (Hyperion Catalysis International, Inc., Japan) named Hyperion Graphite Fibrils, with diameters of 10–20 nm, length of 10–20 μm, and L/D ratio of (1–2) $\times 10^3$ were used in this work. The BET surface area is 250 $m^2 g^{-1}$. The true density is 2.0 $g cm^{-3}$.[24] In the experiment, MWCNTs (100 mg) were oxidized in concentrated HNO_3 (50 mL) by refluxing at 140 °C for 4 h. The mixed solution was filtered by using a polytetrafluoroethylene (PTFE) membrane with a pore size of 1 μm. The filtrate was then washed with water several times to remove residual acid and then sintered at 450 °C for 1 h in an oven.

All chemicals used in this paper were reagent grade, including isopropyl alcohol, nitric acid, and other reagents for the synthesis and photovoltaic experiments for the DSCs.

Preparation: MWCNT/TiO_2 nanocomposites were synthesized by a modified acid-catalyzed sol–gel method. Titanium tetraisopropoxide [TTIP, Wako, Japan] was used as the titanium source. The volume ratio was kept at 10:30:2:200 for $Ti(OPri)_4$:IPA:HNO_3:H_2O. Certain amounts of acid-treated MWCNTs were first sonicated in isopropyl alcohol (IPA, 30 mL) for 30 min to disperse them well. Secondly, titanium tetraisopropoxide (10 mL, Wako, 97%) was added to the MWCNT/IPA solution. The mixed solution was again sonicated for 30 min to improve the interaction between the materials. The mixed solution was then added slowly to distilled deionized water (200 mL). The pH of the distilled water was adjusted to 2 by the addition of concentrated HNO_3, while strongly stirring in an ice bath. A gray, milky slurry was formed, filtered, and washed with deionized water and ethanol several times. The gray, milky slurry was then dried at 80 °C for 1 h. A gray precipitate of the nanocomposite precursor [MWCNT/$Ti(OH)_4$] was obtained and sintered at 450 °C for 1 h. Finally, the MWCNT/TiO_2 nanocomposites were obtained. MWCNT/TiO_2 nanocomposites with different weight ratios of MWCNTs were prepared by dispersing the obtained MWCNT/TiO_2 nanocomposites into TiO_2 nanocrystals and are designated as X-MT, where X (0, 0.01, 0.03, 0.06, 0.10, and 0.50%) relates to the weight ratio of the MWCNTs in the nanocomposite.

MWCNT/$TiO_{2-x}N_x$ nanocomposites were synthesized by heating MWCNT/$Ti(OH)_4$ and urea powder at a weight ratio of 1:2.5. The mixed powder was ground until it could be dispersed well, then sintered at 450 °C for 4 h. A yellow green powder of MWCNT/$TiO_{2-x}N_x$ nanocomposites was then obtained. MWCNT/$TiO_{2-x}N_x$ nanocomposites were designated as X-MN, where X (0, 0.03%, 0.06%, and 0.50%) relates to the weight ratio of the MWCNTs in the nanocomposite.

Fabrication of Films: Screen-printable TiO_2 nanocomposite pastes were prepared according to the procedure developed by our group. Briefly, polyethylene glycol (PEG 600) was used as dispersion medium for the pastes.[39] A screen-printing technique was used to fabricate the TiO_2 films. Firstly, the TiO_2 paste was deposited on the fluorine-doped tin oxide conductive glass (Asahi Glass Co., Ltd.; sheet resistance: 10 Ω/sq). Secondly, the film was sintered at 450 °C for 30 min in atmospheric air. It was then immersed in 40 mM $TiCl_4$ solution at 70 °C for 30 min, rinsed with water and ethanol, and sintered at 500 °C for 30 min. After cooling down to 80 °C, the film was dipped in a dye solution of 5×10^{-4} M *cis*-bis(isothiocyanato) bis(2,2′-bipyridyl-4,4′-dicarboxylato)ruthenium(II)bis(tetrabutylammonium) (N719) dissolved in acetonitrile and 4-*tert*-butyl alcohol (volume ratio 1:1) and kept at room temperature overnight. Finally, a dye-sensitized TiO_2 photoelectrode was obtained. The active area of the MWCNT/TiO_2 electrodes is 0.25 cm^{-2}, and the films have a thickness of ca. 13 μm. For the MWCNT/$TiO_{2-x}N_x$ electrodes, the active area is 0.16 cm^{-2}, and the films have a thickness of ca. 13 μm.

DSC Assembly: The dye-sensitized TiO_2 electrode and a platinized counter electrode were assembled to form a solar cell by sandwiching a redox (I^-/I_3^-) electrolyte solution. In this work, the organic electrolyte consisted of 0.03 M I_2, 0.06 M LiI, 0.6 M 1-butyl-3-methylimidazolium iodide (BMII), 0.1 M guanidinium thiocyanate, and 0.5 M 4-*tert*-butylpyridine in acetonitrile.

Characterization: The size of nanocomposite powders and the microstructure of the films were studied by using field-emission scanning electron microscopy (FE-SEM S-4800, Hitachi, Japan). The phase composition and crystallinity of the nanocomposites were determined by XRD (D/MAX-2400, Japan) with Cu-K_α radiation (γ = 0.1541 nm). The crystallite sizes of TiO_2, $TiO_{2-x}N_x$, and 0.50-MT were estimated by Scherrer's equation, i.e. $D = k\lambda_x/\beta\cos 2\theta$, where D represents the crystal size, k is the dimensionless shape factor with a typical value of 0.89, λ is the wavelength of X-ray

irradiation (0.1541 nm for Cu-K_α radiation), β is the full width at half maximum, and θ is Bragg's diffraction angle.

Photoelectrochemical Measurement: Current–voltage curves of the DSCs were obtained by applying external bias to the cell and by measuring the generated photocurrent under white light irradiation with a Keithley digital source meter (Keithley 2601, USA). The intensity of the incident light was 100 mW cm^{-2}, and the instrument was equipped with a 300 W solar simulator (Solar Light Co., Inc., USA) that served as the light source. The photon flux was determined by a power meter (Nova, Ophir Optronics, Ltd., Japan) and a calibration cell (BS-520, s/n 019, Bunkoh-Keiki Co. Ltd., Japan). Measurement of IPCE was carried out by monitoring the photocurrent at different incident wavelengths with a test system (SM-25, Japan). The photoelectrochemical measurements were carried out in a conventional three-electrode electrochemical cell by using TiO_2, MWCNT/TiO_2, and MWCNT/$TiO_{2-x}N_x$ nanocomposites as the working electrode, Pt wire as the counter electrode, and Ag/AgCl electrode as the reference electrode. The light source and intensity were similar to those used for the measurement of current–voltage curves of the DSCs. No bias was applied to the electrodes; the light was turned on and off every 10 s. The electrolyte was a 1 M KOH solution. Electrochemical impedance measurements (EIS) of the solar cells were performed on a Zahner IM6eX system (Zahner, Germany). The frequency range was 0.1–10^6 Hz and the magnitude of the alternative signal was 10 mV. When the EIS measurements were carried out in the dark, the applied potential was 0.75 V. Thales software packed with Zahner IM6eX software was employed to fit the impedance data.

Acknowledgments

This research was supported by the National Natural Science Foundation of China (Grant No. 50773008) and the State Key Laboratory of New Ceramic and Fine Processing (Tsinghua University). This work was also supported by the National High Technology Research and Development Program for Advanced Materials of China (Grant No. 2009AA03Z220) and the Program for Changjiang Scholars and Innovative Research Team in University (IRT0711).

[1] B. O'Regan, M. Grätzel, *Nature* **1991**, *353*, 737–739.
[2] M. K. Nazeeruddin, P. Pechy, T. Renouard, S. M. Zakeeruddin, R. Humphry-Baker, P. Comte, P. Liska, L. Cevey, E. Costa, V. Shklover, L. Spiccia, G. B. Deacon, C. A. Bignozzi, M. Grätzel, *J. Am. Chem. Soc.* **2001**, *123*, 1613–1624.
[3] D. B. Kuang, S. Ito, B. Wenger, C. Klein, J. E. Moser, R. Humphry-Baker, S. M. Zakeeruddin, M. Grätzel, *J. Am. Chem. Soc.* **2006**, *128*, 4146–4154.
[4] L. Han, A. Fukui, Y. Chiba, A. Islam, R. Komiya, N. Fuke, N. Koide, R. Yamanaka, M. Shimizu, *Appl. Phys. Lett.* **2009**, *94*, 013305.
[5] J. Goldstein, I. Yakupov, B. Breen, *Sol. Energy Mater. Sol. Cells* **2010**, *94*, 638–641.
[6] P. Avouris, M. Freitag, V. Perebeinos, *Nat. Photonics* **2008**, *2*, 341–350.
[7] D. J. Yang, Q. Zhang, G. Chen, S. F. Yoon, J. Ahn, S. G. Wang, Q. Zhou, Q. Wang, J. Q. Li, *Phys. Rev. B* **2002**, *66*, 165440.
[8] T. Umeyamaa, H. Imahori, *Energy Environ. Sci.* **2008**, *1*, 120–133.
[9] E. Kymakis, G. A. J. Amaratunga, *Sol. Energy Mater. Sol. Cells* **2003**, *80*, 465–472.
[10] S. L. Kim, S. R. Jang, R. Vittal, J. Lee, K. J. Kim, *J. Appl. Electrochem.* **2006**, *36*, 1433–1439.
[11] A. Kongkanand, R. M. Domínguez, P. V. Kamat, *Nano Lett.* **2007**, *7*, 676–680.
[12] P. Brown, K. Takechi, P. V. Kamat, *J. Phys. Chem. C* **2008**, *112*, 4776–4782.
[13] T. Y. Lee, P. S. Alegaonkar, J.-B. Yoo, *Thin Solid Films* **2007**, *515*, 5131–5135.
[14] C. Y. Yen, Y. F. Lin, S. H. Liao, C. C. Weng, C. C. Huang, Y. H. Hsiao, C. C. Ma, M. C. Chang, H. Shao, M. C. Tsai, C. K. Hsieh, C. H. Tsai, F. B. Weng, *Nanotechnology* **2008**, *19*, 375305–375314.
[15] T. Sawatsuk, A. Chindaduang, C. Sae-Kung, S. Pratontep, G. Tumcharern, *Diamond Relat. Mater.* **2009**, *18*, 524–527.
[16] J. Liu, Y. Kuo, K. J. Klabunde, C. Rochford, J. Wu, J. Li, *ACS Appl. Mater. Interfaces* **2009**, *1*, 1645–1649.
[17] S. Muduli, W. Lee, V. Dhas, S. Mujawar, M. Dubey, K. Vijayamohanan, S. H. Han, S. Ogale, *ACS Appl. Mater. Interfaces* **2009**, *1*, 2030–2035.
[18] K. M. Lee, C. W. Hu, H. W. Chen, K. C. Ho, *Sol. Energy Mater. Sol. Cells* **2008**, *92*, 1628–1633.
[19] T. Ma, M. Akiyama, E. Abe, I. Imai, *Nano Lett.* **2005**, *5*, 2543–2547.
[20] T. López-Luke, A. Wolcott, L. Xu, S. Chen, Z. Wen, J. Li, E. D. L. Rosa, J. Z. Zhang, *J. Phys. Chem. C* **2008**, *112*, 1282–1292.
[21] T. Lindgren, J. M. Mwabora, E. Avendaño, J. Jonsson, A. Hoel, C. G. Granqvist, S. E. Lindquist, *J. Phys. Chem. B* **2003**, *107*, 5709–5716.
[22] X. Wang, Y. Yang, Z. Jiang, R. Fan, *Eur. J. Inorg. Chem.* **2009**, 3481–3487.
[23] H. Tian, L. Hu, C. Zhang, W. Liu, Y. Huang, L. Mo, L. Guo, J. Sheng, S. Dai, *J. Phys. Chem. C* **2010**, *114*, 1627–1632.
[24] Y. Bin, M. Kitanaka, D. Zhu, M. Matsuo, *Macromolecules* **2003**, *36*, 6213–6219.
[25] R. J. Nemanish, S. A. Solin, *Phys. Rev. B* **1979**, *20*, 392–401.
[26] H. Ago, T. Kugler, F. Cacialli, W. R. Salaneck, M. S. P. Shaffer, A. H. Windle, R. H. Friend, *J. Phys. Chem. B* **1999**, *103*, 8116–8121.
[27] S. W. Lee, W. M. Sigmund, *Chem. Commun.* **2003**, 780–781.
[28] K. P. Wang, H. Teng, *Phys. Chem. Chem. Phys.* **2009**, *11*, 9489–9496.
[29] W. Guo, L. Wu, Z. Chen, T. Ma, G. Boschloo, A. Hagfeldt, *J. Photochem. Photobiol. A* **2011**, DOI: 10.1016/j.jphotochem.2011.01.004.
[30] S. Ito, P. Liska, P. Comte, R. Charvet, P. Péchy, U. Bach, L. Schmidt-Mende, S. M. Zakeeruddin, A. Kay, M. K. Nazeeruddin, M. Grätzel, *Chem. Commun.* **2005**, 4351–4353.
[31] X. Cui, M. Ma, W. Zhang, Y. Yang, Z. Zhang, *Electrochem. Commun.* **2008**, *10*, 367–371.
[32] Q. Wang, J. E. Moser, M. Grätzel, *J. Phys. Chem. B* **2005**, *109*, 14945–14953.
[33] R. Kern, R. Sastrawan, J. Ferber, R. Stangl, J. Luther, *Electrochim. Acta* **2002**, *47*, 4213–4225.
[34] M. Adachi, M. Sakamoto, J. Jiu, Y. Ogata, S. Isoda, *J. Phys. Chem. B* **2006**, *110*, 13872–13880.
[35] S. E. Koops, B. C. O'Regan, P. R. F. Barnes, J. R. Durrant, *J. Am. Chem. Soc.* **2009**, *131*, 4808–4818.
[36] A. Zaban, M. Greenshtein, J. Bisquert, *ChemPhysChem* **2003**, *4*, 859–864.
[37] L. Peter, *Acc. Chem. Res.* **2009**, *42*, 1839–1847.
[38] Q. Wang, Z. Zhang, S. M. Zakeeruddin, M. Grätzel, *J. Phys. Chem. C* **2008**, *112*, 7084–7092.
[39] T. Ma, T. Kida, M. Akiyama, K. Inoue, S. Tsunematsu, K. Yao, H. Noma, E. Abe, *Electrochem. Commun.* **2003**, *5*, 369–372.

Received: November 26, 2010
Published Online: March 4, 2011

